Critical phonon frequency renormalization and dual phonon coexistence in layered Ruddlesden-Popper inorganic perovskites

Zezhu Zeng [1,*] Chen Chen,[1,*] Cunzhi Zhang,[2,*] Qian Zhang,[3] and Yue Chen[1,4,†]

[1]*Department of Mechanical Engineering, The University of Hong Kong, Pokfulam Road, Hong Kong SAR, China*
[2]*Pritzker School of Molecular Engineering, The University of Chicago, Chicago, Illinois, USA*
[3]*School of Materials Science and Engineering, Harbin Institute of Technology, Shenzhen 518055, China*
[4]*HKU Zhejiang Institute of Research and Innovation, 1623 Dayuan Road, Lin An 311305, China*

Phonon-related behaviors such as hot-carrier bottleneck and thermooptic coefficients stimulate the study of lattice dynamics and thermal conductivity (κ) in perovskites. Herein, we report ultralow thermal conductivities of synthesized highly oriented samples of $Cs_2PbI_2Cl_2$ (~ 0.45 W/mK at 300 K) and $Cs_2SnI_2Cl_2$ (~ 0.60 W/mK at 300 K). Phonon frequency renormalization of the octahedral rotational soft modes in $Cs_2PbI_2Cl_2$ triggered by the fourth-order anharmonicity considerably amends the three- and four-phonon linewidths, significantly altering the thermal transport property of $Cs_2PbI_2Cl_2$. Furthermore, the phonon gas model partially breaks down, and both normal and diffuson-like phonons must be considered to capture the nearly temperature-independent κ of $Cs_2PbI_2Cl_2$. We also find these unusual phonon behaviors in other layered inorganic perovskites such as $Cs_2PbBr_2Cl_2$ and $Cs_2SnI_2Cl_2$. Our results rationalize the crucial high-order phonon interactions and two-channel lattice thermal transports in perovskites with ultralow κ.

I. INTRODUCTION

Effective manipulation and utilization of heat energy is crucial to photovoltaics and optoelectronics as their performance and lifetime are influenced by the temperature gradients generated during operation [1,2]. Phonon, as a lattice thermal excitation, plays a critical role to determine the lattice thermal conductivity (κ) of materials, and affects the efficiency and property of perovskites-based devices. For instance, the hot-phonon bottleneck effect in lead-halide perovskites [3] significantly prolongs the cooling period of charge carriers [4,5]. Some halide perovskites [6–9] are promising thermoelectric materials owing to their ultralow κ and favorable electrical properties. On the other hand, perovskites with relatively high κ can dissipate heat efficiently and thus increase the lifetime of microelectronic devices. This wide-scale interest in the thermal energy field leads to an urgent requirement of understanding the lattice dynamics of perovskites. Nevertheless, exhaustive investigations of phonon thermal transport in perovskites are rare [10], mainly attributing to the complicated crystal structures and strong lattice anharmonicity. Despite some experimental studies [6,11–13] of the thermal transport behaviors of perovskites and their effects on the optoelectronic properties, the theoretical horizons about the nature of the complex thermal property of perovskites are still in its infancy.

Two-dimensional (2D) perovskites [14–19] have emerged as a new class of materials attractive for their excellent stability and superior optoelectronic properties. In particular, all-inorganic layered Ruddlesden-Popper (RP) perovskites ($Cs_2XY_2Cl_2$; X = Pb, Sn; Y = I, Br), as outstanding candidates within the 2D perovskite family, have been extensively studied [16,20–28]. However, its complex lattice dynamics and heat transport that are closely related to its optoelectronic properties are yet to be further explored. Acharyya *et al.* [29] first reported that 2D RP inorganic perovskite $Cs_2PbI_2Cl_2$ displays an ultralow thermal conductivity of 0.37 W/mK at 300 K, which is even lower than those of the halide perovskites $CsPbI_3$ (0.45 W/mK) and $CsPbBr_3$ (0.42 W/mK) [13]. The ultralow κ was discussed based on the harmonic phonons at 0 K [29], while the temperature-dependent anharmonic phonon interactions were ignored. Moreover, cubic and higher-order lattice anharmonicity may be crucial for the thermal transport behavior of complex materials at elevated temperatures [30–36]. For example, Klarbring *et al.* [37] reported significant fourth-order anharmonicity in halide perovskite $Cs_2AgBiBr_6$.

Herein, we thoroughly investigate the lattice dynamics of 2D RP inorganic perovskites utilizing the first-principles-based calculations in conjunction with experimental measurements. We synthesize two high-quality polycrystalline samples ($Cs_2PbI_2Cl_2$ and $Cs_2SnI_2Cl_2$) and measure their thermal conductivities at different temperatures. Our calculations indicate that strong high-order anharmonic renormalization significantly lifts the frequencies of the dynamic octahedral soft modes in $Cs_2PbI_2Cl_2$ and thus inhibits the acoustic-optical phonon interactions, which considerably amends the phonon linewidths and κ. Moreover, significant four-phonon interactions are found in $Cs_2PbI_2Cl_2$, contributing to the ultralow κ at room temperature. In addition, strong

*These authors contributed equally to this work.
†yuechen@hku.hk
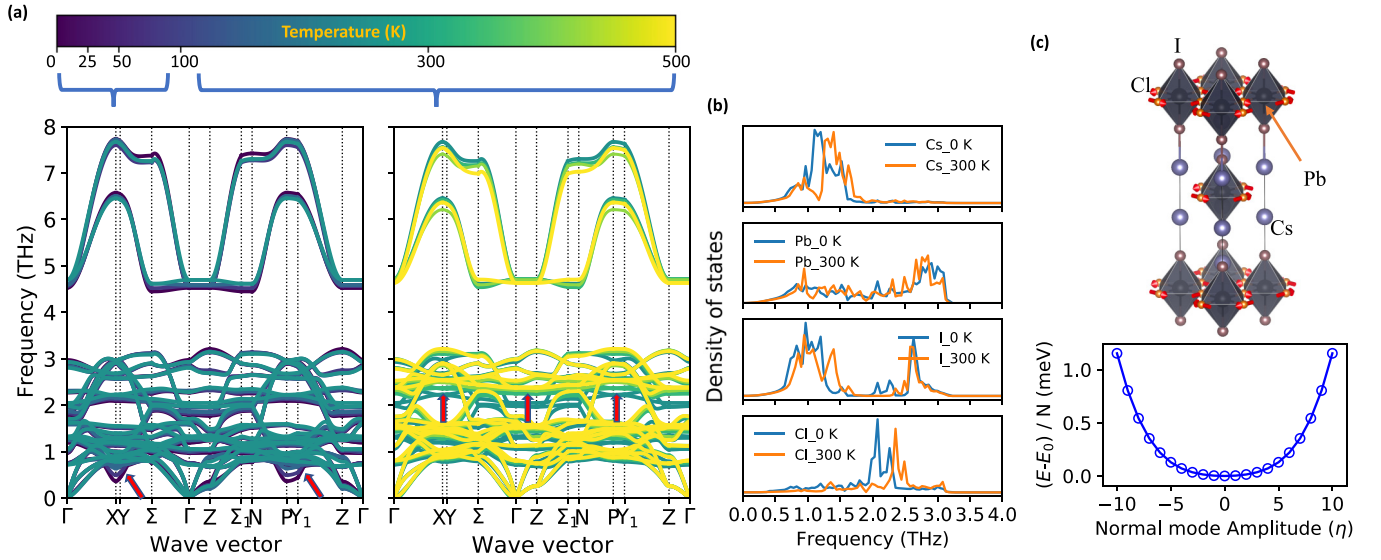
FIG. 1. (a) Temperature-dependent phonon dispersions of $Cs_2PbI_2Cl_2$ calculated using the temperature-dependent effective potential [39–41] scheme. (b) Projected density of states of $Cs_2PbI_2Cl_2$ calculated at 0 K and 300 K. (c) Visualization [52] of the lowest-frequency phonon mode at X point and its potential energy surface calculated from DFT using VASP [53]. The arrows represent the rotational directions of Cl atoms.

lattice anharmonicity breaks down the conventional phonon-gas picture, and both normal and diffuson-like phonons must be considered to capture the dual phonon [38] thermal transport behavior. We demonstrate that our findings are also applicative in other 2D RP inorganic perovskites such as $Cs_2SnI_2Cl_2$ and $Cs_2PbBr_2Cl_2$.

II. RESULTS AND DISCUSSION

We first study the anharmonic phonon frequency renormalization of $Cs_2PbI_2Cl_2$ using the temperature-dependent effective potential (TDEP) [39–41] scheme (see Supplemental Material [42] for more details [43–51]), and the result is shown in Fig. 1(a). At 0 K, we observe a similar soft mode at the X point with a frequency of ~ 0.36 THz as that reported by Acharyya *et al.* [29]. This soft mode is usually related to ultralow-κ property of materials as it facilitates adequate scatterings of the heat-carrying acoustic phonons. Interestingly, we observe a notable hardening of this soft mode and the optical modes at ~ 2 THz at elevated temperatures. From the results of the projected density of states of Cl element as shown in Fig. 1(b), we can also see an obvious shift of the peak at ~ 2 THz towards a higher frequency region when temperature increases.

We further comprehend this significant frequency renormalization by analyzing the local potential energy surface (PES) [30,54–56]. The lowest-frequency phonon mode at the X point corresponds to the dynamic octahedral rotation of Cl atoms around the octahedral centers occupied by Pb atoms. We calculate the PES of this soft mode and a symmetric U-type PES [Fig. 1(c)] is observed, suggesting strong quartic lattice anharmonicity [30,56,57]. The vibrational atoms related to this mode can move away easily from the equilibrium positions as the PES is shallow [56,57], which also suggests that the conventional harmonic approximation with

small atomic displacements cannot effectively capture the strongly anharmonic lattice dynamics of $Cs_2PbI_2Cl_2$ [30,31].

Renormalized phonon dispersions lead to different phonon scattering phase space [58,59] and further affect the phonon scattering rates. The acoustic-optical phonon interactions are especially sensitive to the renormalization of the low-frequency phonon modes [30,60,61]. We investigate the influence of phonon frequency renormalization on the three-phonon (3ph) and four-phonon (4ph) linewidths at 300 K [62–64] (see SM for calculation details). Large differences of an order of magnitude are found for the 3ph [Fig. 2(a)] and 4ph [Fig. 2(b)] linewidths in the low-frequency region around 1 THz, indicating the phonon frequency renormalization is critical for accurate phonon linewidths calculations. Comparing the 3ph and 4ph linewidths calculated with the phonon frequency renormalization, we also reveal the importance of 4ph interactions in further decreasing the κ (see Fig. S6 of SM). The large 4ph linewidths ($10 \sim 10^2$ ps^{-1}) of the low frequency phonons in Fig. 2(b) can be attributed to the strong redistribution processes of the phonon modes with wave vectors near the vicinity of P and Y_1 high-symmetry points (see Figs. S12 and S13).

The anharmonic renormalization remarkably influences the phonon frequencies and linewidths, inevitably having crucial effects on the κ [59]. As $Cs_2PbI_2Cl_2$ is anisotropic, the lattice thermal conductivities along x ($\kappa_x = \kappa_y$) and z directions are calculated [see Figs. 2(d) and 2(e)] based on the conventional phonon Boltzmann transport equation [65,66] on top of fixed second-order IFCs at 0 K (no frequency renormalization) and temperature-dependent second-order IFCs (with frequency renormalization). It is noted that the cubic and quartic IFCs are both temperature dependent in all our calculations. A high-quality polycrystal sample of $Cs_2PbI_2Cl_2$ is synthesized using the annealing and spark plasma sintering (SPS) method (see SM for the experimental details and XRD results), and the thermal conductivities along the parallel and perpendicular
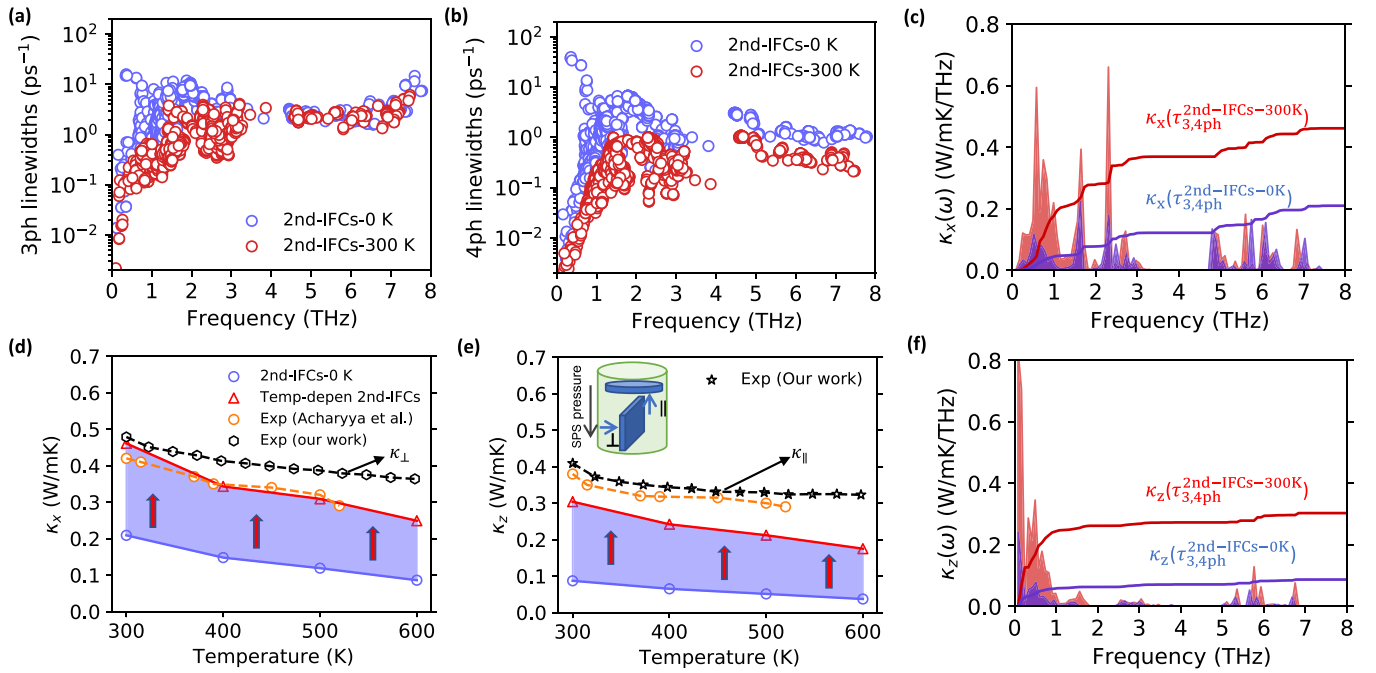
FIG. 2. (a) Three-phonon (3ph) and (b) four-phonon (4ph) linewidths at 300 K calculated using two different sets of second-order inter-atomic force constants (IFCs); second-IFCs-0K is obtained with the small displacement method, and second-IFCs-300 K is the renormalized values at 300 K obtained based on the TDEP scheme. (d,e) Theoretical (conventional phonon gas model considering 3ph and 4ph interactions) and experimental results of the lattice thermal conductivities of $Cs_2PbI_2Cl_2$ along different directions. The blue shaded regions represent the crucial effects of phonon frequency renormalization on the calculated κ. A schematic diagram of our sample and the measured directions of thermal conductivities are shown in (e). Frequency-dependent spectral lattice thermal conductivities at 300 K along (c) x and (f) z directions as calculated using second-IFCs-0 K and second-IFCs-300 K. Both 3ph and 4ph interactions are considered.

directions of SPS pressure are measured. Our measured κ is similar to the results reported by Acharyya *et al.* [29] based on samples synthesized using the Bridgman method. We measure the resistivity of the sample and find the material is noncon-ducting, thus the measured thermal conductivity (κ) can be considered as the lattice thermal conductivity ($\kappa_L = \kappa$). The optical absorption spectrum (see Fig. S2 of SM) also indicates $Cs_2PbI_2Cl_2$ is an insulator with a large band gap of 2.9 eV.

Notably, the calculated κ_x and κ_z raise significantly after considering the phonon frequency renormalization [see the blue regions in Figs. 2(d) and 2(e) for the enhancement]. For example, at 600 K, κ_z computed with phonon renormal-ization is equal to 0.175 W/mK, which is about five times larger than that (0.037 W/mK) calculated based on the har-monic phonon frequency at 0 K. These results demonstrate the significance of phonon frequency renormalization in the correct description of the heat transport of $Cs_2PbI_2Cl_2$. The phonon group velocities calculated using the second-order atomic force constants at 0 K and the renormalized values at 300 K are compared (see Fig. S7 of SM), but no distinct dif-ference is identified. In contrast, from Figs. 2(a) and 2(b), we know that the phonon linewidths of the low-frequency modes largely decrease after considering frequency renormalization; therefore, the decreased phonon linewidths are responsible for the considerable enhancement of the calculated κ. From the spectral lattice thermal conductivities shown in Figs. 2(c) and 2(f), it is also evident that phonon frequency renormalization apparently enhances the heat transport of the low-frequency heat carriers (0–1 THz).

Despite considering the phonon frequency renormaliza-tion, we find that the theoretical κ is still lower than the experimental values, especially for κ_z at high temperatures [see Fig. 2(e)]. Recent advancements [38,67–71] of the unified theory for heat transport of crystals and glasses provide a more sophisticated approach to understand the κ of strongly anharmonic materials. In conventional crystals, the phonon picture is valid as the mean free path of phonons is much larger than the wavelength or the minimum interatomic spac-ing. While for strongly anharmonic materials, the definition of the phonon can become ambiguous. Einstein *et al.* [72,73] pointed out that heat is carried by random walk among un-correlated oscillators. Mukhopadhyay *et al.* [70] provided a two-channel model to describe the thermal transport of com-plex materials by a simple addition of the phonon gas model and the random walk theory. Luo *et al.* [38] further proposed a dual-phonon theory based on the phonon thermal diffusiv-ity: normal phonons described by the Boltzmann transport equation, and diffuson-like phonons described by the diffu-sion theory. In the dual phonon picture, if a vibrational mode is characterized as a normal phonon, it cannot be treated as a diffuson-like phonon at the same time and vice versa (see SM for details).

In Figs. 3(a) and 3(b), we calculate the thermal diffu-sivities of all vibrational modes on top of the renormalized phonon frequencies with 3ph and 4ph linewidths, and make a comparison with the critical criterion of diffuson-like phonon based on the random walk theory [38,74]. We note that the phonon wavelength can also be used as a criterion to obtain
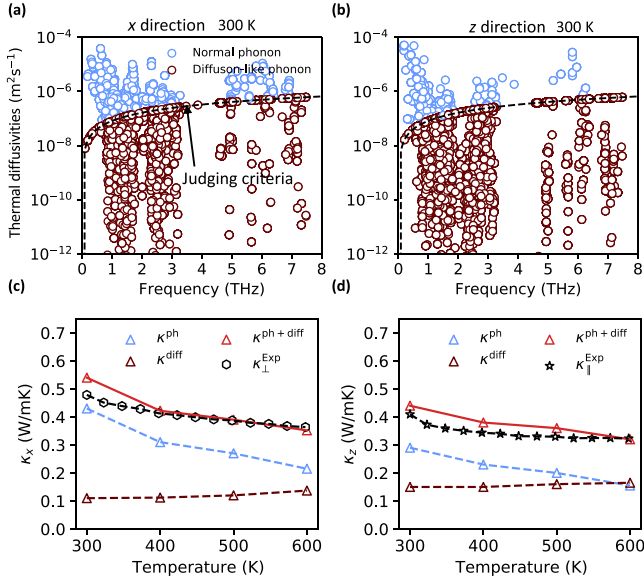
FIG. 3. Thermal diffusivisities of $Cs_2PbI_2Cl_2$ at 300 K along (a) x and (b) z directions calculated using the renormalized second-order IFCs considering both 3ph and 4ph interactions. The black dotted line provides a critical criterion to determine the phonons category based on the random walk theory. (c),(d) Lattice thermal conductivities contributed by the normal phonons (κ^{ph}) and the diffuson-like phonons (κ^{diff}) calculated using the dual phonon theory along different directions.

FIG. 4. Temperature-dependent phonon dispersions calculated using the TDEP scheme for (a) $Cs_2PbBr_2Cl_2$ and (b) $Cs_2SnI_2Cl_2$. Three- and four-phonon linewidths calculated based on the renormalized second-order interatomic force constants at 300 K for (c) $Cs_2PbBr_2Cl_2$ and (d) $Cs_2SnI_2Cl_2$.

similar results (see Fig. S14). We see that many phonons in $Cs_2PbI_2Cl_2$ cannot be defined as normal phonons at 300 K. These diffuson-like phonons with small thermal diffusivities (short phonon mean free paths) can contribute to κ based on the random walk theory [38,74]. Therefore, phonon Boltzmann transport theory is valid for well-defined normal phonons to compute the long-ranged thermal propagation (κ^{ph}), while random walk theory [38,74] can be used to calculate the diffusive transport (κ^{diff}), and the lattice thermal conductivity ($\kappa^{ph+diff}$) is the addition of the dual phonon contributions. We also investigate the effects of the phonon frequency renormalization on the dual phonon category, and the results (see Fig. S8) indicate that it is crucial to differentiate between normal and diffuson-like phonons.

In Figs. 3(c) and 3(d), we find that both κ_x^{ph} and κ_z^{ph} deviate further from the experimental results at high temperatures, suggesting the potential importance of dual phonon transports in $Cs_2PbI_2Cl_2$. Moreover, we find that κ_z^{diff} even surpasses κ_z^{ph} at 600 K, indicating that the diffusive thermal channel can dominate the thermal transport at elevated temperatures. After introducing the diffusive channel, the lattice thermal conductivities ($\kappa^{ph+diff}$) agree well with the experimental results along both directions, demonstrating that the two-channel thermal transports triggered by dual phonons are critical for the description of the thermal property of $Cs_2PbI_2Cl_2$.

The results obtained for $Cs_2PbI_2Cl_2$ can be extended to other 2D RP inorganic perovskites. We take $Cs_2SnI_2Cl_2$ [26,75] and $Cs_2PbBr_2Cl_2$ [76] as examples and find that phonon frequency renormalization, four-phonon interactions (see Fig. 4) and dual phonon transports (see Fig. S9) are also
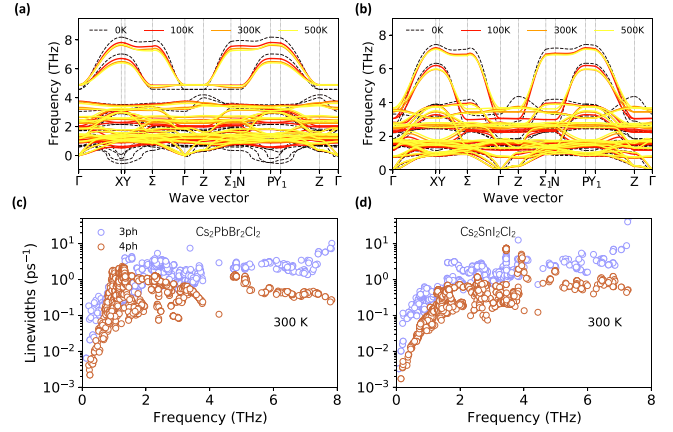
of critical importance for these perovskites. Some phonons exhibit imaginary frequencies at the X point in $Cs_2PbBr_2Cl_2$ at 0 K, which can be eliminated at elevated temperatures owing to phonon frequency renormalization. For $Cs_2PbBr_2Cl_2$, 4ph scatterings even surpass 3ph scatterings in the low-frequency region at 300 K. Strong phonon scatterings considerably decrease the thermal diffusivities and lead to a more significant dual phonon thermal transport behavior. In Fig. 5, we report the strong frequency renormalization effects on κ based on the conventional phonon gas model for $Cs_2PbBr_2Cl_2$ and $Cs_2SnI_2Cl_2$. The lattice thermal conductivities have also been
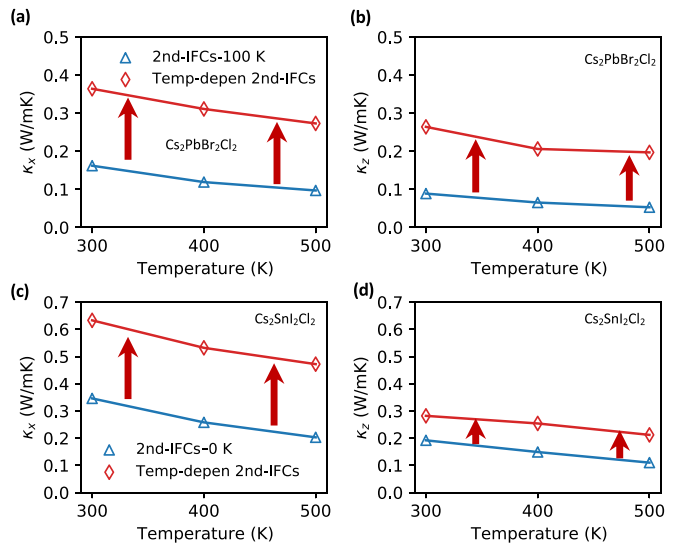
FIG. 5. Effects of phonon frequency renormalization on the lattice thermal conductivities of (a),(b) $Cs_2PbBr_2Cl_2$ and (c),(d) $Cs_2SnI_2Cl_2$ calculated using the conventional phonon gas model. Three- and four-phonon interactions are considered in the calculations. Because the harmonic phonon dispersion at 0 K has imaginary frequencies for $Cs_2PbBr_2Cl_2$, we use the renormalized second-order IFCs at 100 K to perform the calculations.
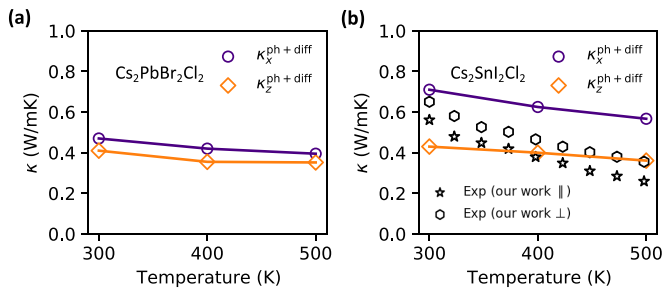
FIG. 6. Lattice thermal conductivities calculated using the dual phonon theory for (a) $Cs_2PbBr_2Cl_2$ and (b) $Cs_2SnI_2Cl_2$. The experimental results of $Cs_2SnI_2Cl_2$ polycrystal are shown for comparison.

calculated using the dual phonon theory [38] and the results are shown in Fig. 6. The individual κ^{ph} and κ^{diff} for these two materials are shown in Fig. S10 of SM. The experimental κ of $Cs_2SnI_2Cl_2$ polycrystal is also included in Fig. 6(b) for comparison. The theoretical κ is in reasonable agreement with the experiment, while the lower experimental κ at high temperatures may result from other sources of phonon scatterings in polycrystals not considered in our single-crystal calculations.

III. CONCLUSION

In summary, the anharmonic lattice dynamics and thermal transport property of 2D RP inorganic perovskites are thoroughly investigated. We reveal that phonon frequency renormalization and strong fourth-order lattice anharmonicity are crucial to correctly comprehend the thermal transport behaviors of 2D RP inorganic perovskites. We find that the nearly temperature-independent κ can be correctly described only when normal and diffuson-like phonons are both taken into account. This work unveils the nature of lattice thermal transport in 2D RP inorganic perovskites and provides potential new avenues for the engineering of the phonon-related properties.

ACKNOWLEDGMENTS

[1] E. Skoplaki and J. A. Palyvos, On the temperature dependence of photovoltaic module electrical performance: A review of efficiency/power correlations, Sol. Energy **83**, 614 (2009).

[2] T. Lanigan-Atkins, X. He, M. Krogstad, D. Pajerowski, D. Abernathy, G. N. Xu, Z. Xu, D.-Y. Chung, M. Kanatzidis, S. Rosenkranz *et al.*, Two-dimensional overdamped fluctuations of the soft perovskite lattice in cspbbr3, Nat. Mater. **20**, 977 (2021).

[3] J. Yang, X. Wen, H. Xia, R. Sheng, Q. Ma, J. Kim, P. Tapping, T. Harada, T. W. Kee, F. Huang *et al.*, Acoustic-optical phonon up-conversion and hot-phonon bottleneck in lead-halide perovskites, Nat. Commun. **8**, 1 (2017).

[4] Y. Yang, D. P. Ostrowski, R. M. France, K. Zhu, J. Van De Lagemaat, J. M. Luther, and M. C. Beard, Observation of a hot-phonon bottleneck in lead-iodide perovskites, Nat. Photonics **10**, 53 (2016).

[5] X. Jia, J. Jiang, Y. Zhang, J. Qiu, S. Wang, Z. Chen, N. Yuan, and J. Ding, Observation of enhanced hot phonon bottleneck effect in 2D perovskites, Appl. Phys. Lett. **112**, 143903 (2018).

[6] H. Xie, S. Hao, J. Bao, T. J. Slade, G. J. Snyder, C. Wolverton, and M. G. Kanatzidis, All-inorganic halide perovskites as potential thermoelectric materials: Dynamic cation off-centering induces ultralow thermal conductivity, J. Am. Chem. Soc. **142**, 9553 (2020).

[7] T. Liu, X. Zhao, J. Li, Z. Liu, F. Liscio, S. Milita, B. C. Schroeder, and O. Fenwick, Enhanced control of self-doping in halide perovskites for improved thermoelectric performance, Nat. Commun. **10**, 1 (2019).

[8] J. He and T. M. Tritt, Advances in thermoelectric materials research: Looking back and moving forward, Science **357**, eaak9997 (2017).

[9] M. A. Haque, S. Kee, D. R. Villalva, W.-L. Ong, and D. Baran, Halide perovskites: Thermal transport and prospects for thermoelectricity, Adv. Sci. **7**, 1903389 (2020).

[10] M. Menahem, Z. Dai, S. Aharon, R. Sharma, M. Asher, Y. Diskin-Posner, R. Korobko, A. M. Rappe, and O. Yaffe, Strongly anharmonic octahedral tilting in two-dimensional hybrid halide perovskites, ACS Nano **15**, 10153 (2021).

[11] A. D. Christodoulides, P. Guo, L. Dai, J. M. Hoffman, X. Li, X. Zuo, D. Rosenmann, A. Brumberg, M. G. Kanatzidis, R. D. Schaller *et al.*, Signatures of coherent phonon transport in ultralow thermal conductivity two-dimensional Ruddlesden-Popper phase perovskites, ACS Nano **15**, 4165 (2021).

[12] A. Ferreira, S. Paofai, A. Létoublon, J. Ollivier, S. Raymond, B. Hehlen, B. Rufflé, S. Cordier, C. Katan, J. Even *et al.*, Direct evidence of weakly dispersed and strongly anharmonic optical phonons in hybrid perovskites, Commun. Phys. **3**, 48 (2020).

[13] W. Lee, H. Li, A. B. Wong, D. Zhang, M. Lai, Y. Yu, Q. Kong, E. Lin, J. J. Urban, J. C. Grossman *et al.*, Ultralow thermal conductivity in all-inorganic halide perovskites, Proc. Natl. Acad. Sci. **114**, 8693 (2017).

[14] L. Mao, C. C. Stoumpos, and M. G. Kanatzidis, Two-dimensional hybrid halide perovskites: Principles and promises, J. Am. Chem. Soc. **141**, 1171 (2019).

[15] A. Biswas, R. Bakthavatsalam, and J. Kundu, Efficient exciton to dopant energy transfer in Mn^{2+}-doped $(C_4H_9NH_3)_2PbBr_4$ two-dimensional (2D) layered perovskites, Chem. Mater. **29**, 7816 (2017).

[16] H. Tsai, W. Nie, J.-C. Blancon, C. C. Stoumpos, R. Asadpour, B. Harutyunyan, A. J. Neukirch, R. Verduzco, J. J. Crochet, S. Tretiak *et al.*, High-efficiency two-dimensional Ruddlesden-Popper perovskite solar cells, Nature (London) **536**, 312 (2016).

[17] Y. Chen, S. Yu, S. Sun, and Z. Liang, Phase engineering in quasi-2D Ruddlesden-Popper perovskites, J. Phys. Chem. Lett. **9**, 2627 (2018).

[18] H. A. Evans, L. Mao, R. Seshadri, and A. K. Cheetham, Layered double perovskites, Annu. Rev. Mater. Res. **51**, 351 (2021).

[19] L.-F. Huang, X.-Z. Lu, and J. M. Rondinelli, Tunable Negative Thermal Expansion in Layered Perovskites from Quasi-Two-Dimensional Vibrations, Phys. Rev. Lett. **117**, 115901 (2016).

[20] L.-Y. Pan, Y.-F. Ding, Z.-L. Yu, Q. Wan, B. Liu, and M.-Q. Cai, Layer-dependent optoelectronic property for all-inorganic two-dimensional mixed halide perovskite $Cs_2PbI_2Cl_2$ with a Ruddlesden-Popper structure, J. Power Sources **451**, 227732 (2020).

[21] S. Yang, W. Liu, Y. Han, Z. Liu, W. Zhao, C. Duan, Y. Che, H. Gu, Y. Li, and S. Liu, 2D $Cs_2PbI_2Cl_2$ nanosheets for holistic passivation of inorganic $CsPbI_2Br$ perovskite solar cells for improved efficiency and stability, Adv. Energy Mater. **10**, 2002882 (2020).

[22] Y. Yu, D. Zhang, and P. Yang, Ruddlesden–Popper phase in two-dimensional inorganic halide perovskites: A plausible model and the supporting observations, Nano Lett. **17**, 5489 (2017).

[23] J. Li, Q. Yu, Y. He, C. C. Stoumpos, G. Niu, G. G. Trimarchi, H. Guo, G. Dong, D. Wang, L. Wang *et al.*, $Cs_2PbI_2Cl_2$, all-inorganic two-dimensional Ruddlesden-Popper mixed halide perovskite with optoelectronic response, J. Am. Chem. Soc. **140**, 11085 (2018).

[24] P. Maity, J. Yin, B. Cheng, J.-H. He, O. M. Bakr, and O. F. Mohammed, Layer-dependent coherent acoustic phonons in two-dimensional Ruddlesden-Popper perovskite crystals, J. Phys. Chem. Lett. **10**, 5259 (2019).

[25] D. Pan, Y. Fu, N. Spitha, Y. Zhao, C. R. Roy, D. J. Morrow, D. D. Kohler, J. C. Wright, and S. Jin, Deterministic fabrication of arbitrary vertical heterostructures of two-dimensional Ruddlesden-Popper halide perovskites, Nat. Nanotechnol. **16**, 159 (2021).

[26] Z. Xu, M. Chen, and S. F. Liu, Layer-dependent ultrahigh-mobility transport properties in all-inorganic two-dimensional $Cs_2PbI_2Cl_2$ and $Cs_2SnI_2Cl_2$ perovskites, J. Phys. Chem. C **123**, 27978 (2019).

[27] P. Acharyya, K. Kundu, and K. Biswas, 2D layered all-inorganic halide perovskites: Recent trends in their structure, synthesis and properties, Nanoscale **12**, 21094 (2020).

[28] K. Kundu, P. Dutta, P. Acharyya, and K. Biswas, Mechanochemical synthesis, optical and magnetic properties of Pb-free Ruddlesden–Popper-Type layered $Rb_2CuCl_2Br_2$ perovskite, J. Phys. Chem. C **125**, 4720 (2021).

[29] P. Acharyya, T. Ghosh, K. Pal, K. Kundu, K. Singh Rana, J. Pandey, A. Soni, U. V. Waghmare, and K. Biswas, Intrinsically ultralow thermal conductivity in Ruddlesden-Popper 2D perovskite $Cs_2PbI_2Cl_2$: Localized anharmonic vibrations and dynamic octahedral distortions, J. Am. Chem. Soc. **142**, 15595 (2020).

[30] Y. Xia, K. Pal, J. He, V. Ozoliņš, and C. Wolverton, Particlelike Phonon Propagation Dominates Ultralow Lattice Thermal Conductivity in Crystalline Tl_3VSe_4, Phys. Rev. Lett. **124**, 065901 (2020).

[31] Z. Zeng, C. Zhang, Y. Xia, Z. Fan, C. Wolverton, and Y. Chen, Nonperturbative phonon scatterings and the two-channel thermal transport in Tl_3VSe_4, Phys. Rev. B **103**, 224307 (2021).

[32] T. Tadano and S. Tsuneyuki, Self-consistent phonon calculations of lattice dynamical properties in cubic $SrTiO_3$ with first-principles anharmonic force constants, Phys. Rev. B **92**, 054301 (2015).

[33] Z. Zeng, C. Zhang, H. Yu, W. Li, Y. Pei, and Y. Chen, Ultralow and glass-like lattice thermal conductivity in crystalline $BaAg_2Te_2$: Strong fourth-order anharmonicity and crucial diffusive thermal transport, Mater. Today Phys. **21**, 100487 (2021).

[34] L. Paulatto, I. Errea, M. Calandra, and F. Mauri, First-principles calculations of phonon frequencies, lifetimes, and spectral functions from weak to strong anharmonicity: The example of palladium hydrides, Phys. Rev. B **91**, 054304 (2015).

[35] X. He, D. Bansal, B. Winn, S. Chi, L. Boatner, and O. Delaire, Anharmonic Eigenvectors and Acoustic Phonon Disappearance in Quantum Paraelectric $SrTiO_3$, Phys. Rev. Lett. **124**, 145901 (2020).

[36] C. Zhang, Z. Zeng, Q. Sun, and Y. Chen, Stronger three-phonon interactions revealed by molecular dynamics in materials with restricted phase space, J. Appl. Phys. **130**, 205101 (2021).

[37] J. Klarbring, O. Hellman, I. A. Abrikosov, and S. I. Simak, Anharmonicity and Ultralow Thermal Conductivity in Lead-Free Halide Double Perovskites, Phys. Rev. Lett. **125**, 045701 (2020).

[38] Y. Luo, X. Yang, T. Feng, J. Wang, and X. Ruan, Vibrational hierarchy leads to dual-phonon transport in low thermal conductivity crystals, Nat. Commun. **11**, 1 (2020).

[39] O. Hellman, I. A. Abrikosov, and S. I. Simak, Lattice dynamics of anharmonic solids from first principles, Phys. Rev. B **84**, 180301(R) (2011).

[40] O. Hellman, P. Steneteg, I. A. Abrikosov, and S. I. Simak, Temperature dependent effective potential method for accurate free energy calculations of solids, Phys. Rev. B **87**, 104111 (2013).

[41] O. Hellman and I. A. Abrikosov, Temperature-dependent effective third-order interatomic force constants from first principles, Phys. Rev. B **88**, 144301 (2013).

[42] See Supplemental Material at http://link.aps.org/supplemental/10.1103/PhysRevB.105.184303 for experimental and calculated details.

[43] J. P. Perdew, A. Ruzsinszky, G. I. Csonka, O. A. Vydrov, G. E. Scuseria, L. A. Constantin, X. Zhou, and K. Burke, Restoring the Density-Gradient Expansion for Exchange in Solids and Surfaces, Phys. Rev. Lett. **100**, 136406 (2008).

[44] L.-D. Zhao, S.-H. Lo, Y. Zhang, H. Sun, G. Tan, C. Uher, C. Wolverton, V. P. Dravid, and M. G. Kanatzidis, Ultralow thermal conductivity and high thermoelectric figure of merit in SnSe crystals, Nature (London) **508**, 373 (2014).

[45] J. C. Jaeger and H. S. Carslaw, *Conduction of Heat in Solids* (Clarendon, New York, 1959).

[46] P. E. Blöchl, Projector augmented-wave method, Phys. Rev. B **50**, 17953 (1994).

[47] J. Shuai, Y. Wang, H. S. Kim, Z. Liu, J. Sun, S. Chen, J. Sui, and Z. Ren, Thermoelectric properties of na-doped zintl compound: $Mg_{3-x}Na_xSb_2$, Acta Mater. **93**, 187 (2015).

[48] Y. Luo, S. Cai, S. Hao, F. Pielnhofer, I. Hadar, Z.-Z. Luo, J. Xu, C. Wolverton, V. P. Dravid, A. Pfitzner *et al.*, High-performance thermoelectrics from cellular nanostructured $Sb_2Si_2Te_6$, Joule **4**, 159 (2020).

[49] A. Togo and I. Tanaka, First principles phonon calculations in materials science, Scr. Mater. **108**, 1 (2015).

[50] W. Li, J. Carrete, N. A. Katcho, and N. Mingo, ShengBTE: A solver of the boltzmann transport equation for phonons, Comput. Phys. Commun. **185**, 1747 (2014).

[51] F. Eriksson, E. Fransson, and P. Erhart, The hiphive package for the extraction of high-order force constants by machine learning, Adv. Theory Simul. **2**, 1800184 (2019).

[52] K. Momma and F. Izumi, VESTA 3 for three-dimensional visualization of crystal, volumetric and morphology data, J. Appl. Crystallogr. **44**, 1272 (2011).

[53] G. Kresse and J. Furthmüller, Efficient iterative schemes for ab initio total-energy calculations using a plane-wave basis set, Phys. Rev. B **54**, 11169 (1996).

[54] M. Dutta, S. Matteppanavar, M. V. Prasad, J. Pandey, A. Warankar, P. Mandal, A. Soni, U. V. Waghmare, and K. Biswas, Ultralow thermal conductivity in chain-like TlSe due to inherent Tl^+ rattling, J. Am. Chem. Soc. **141**, 20293 (2019).

[55] Z. Zeng, S. Li, T. Tadano, and Y. Chen, Anharmonic lattice dynamics and thermal transport of monolayer InSe under equibiaxial tensile strains, J. Phys.: Condens. Matter **32**, 475702 (2020).

[56] T. Tadano and S. Tsuneyuki, Quartic Anharmonicity of Rattlers and Its Effect on Lattice Thermal Conductivity of Clathrates from First Principles, Phys. Rev. Lett. **120**, 105901 (2018).

[57] S.-Y. Yue, X. Zhang, G. Qin, S. R. Phillpot, and M. Hu, Metric for strong intrinsic fourth-order phonon anharmonicity, Phys. Rev. B **95**, 195203 (2017).

[58] L. Lindsay and D. Broido, Three-phonon phase space and lattice thermal conductivity in semiconductors, J. Phys.: Condens. Matter **20**, 165209 (2008).

[59] Q. Wang, Z. Zeng, and Y. Chen, Revisiting phonon transport in perovskite $SrTiO_3$: Anharmonic phonon renormalization and four-phonon scattering, Phys. Rev. B **104**, 235205 (2021).

[60] A. Jain, Multichannel thermal transport in crystalline Tl_3VSe_4, Phys. Rev. B **102**, 201201(R) (2020).

[61] N. K. Ravichandran and D. Broido, Unified first-principles theory of thermal properties of insulators, Phys. Rev. B **98**, 085205 (2018).

[62] T. Feng and X. Ruan, Quantum mechanical prediction of four-phonon scattering rates and reduced thermal conductivity of solids, Phys. Rev. B **93**, 045202 (2016).

[63] T. Feng, L. Lindsay, and X. Ruan, Four-phonon scattering significantly reduces intrinsic thermal conductivity of solids, Phys. Rev. B **96**, 161201(R) (2017).

[64] T. Feng and X. Ruan, Four-phonon scattering reduces intrinsic thermal conductivity of graphene and the contributions from flexural phonons, Phys. Rev. B **97**, 045202 (2018).

[65] A. Togo, L. Chaput, and I. Tanaka, Distributions of phonon lifetimes in brillouin zones, Phys. Rev. B **91**, 094306 (2015).

[66] L. Lindsay, A. Katre, A. Cepellotti, and N. Mingo, Perspective on *ab initio* phonon thermal transport, J. Appl. Phys. **126**, 050902 (2019).

[67] M. Simoncelli, N. Marzari, and F. Mauri, Unified theory of thermal transport in crystals and glasses, Nat. Phys. **15**, 809 (2019).

[68] L. Isaeva, G. Barbalinardo, D. Donadio, and S. Baroni, Modeling heat transport in crystals and glasses from a unified lattice-dynamical approach, Nat. Commun. **10**, 3853 (2019).

[69] R. Hanus, J. George, M. Wood, A. Bonkowski, Y. Cheng, D. L. Abernathy, M. E. Manley, G. Hautier, G. J. Snyder, and R. P. Hermann, Uncovering design principles for amorphous-like heat conduction using two-channel lattice dynamics, Mater. Today Phys. **18**, 100344 (2021).

[70] S. Mukhopadhyay, D. S. Parker, B. C. Sales, A. A. Puretzky, M. A. McGuire, and L. Lindsay, Two-channel model for ultralow thermal conductivity of crystalline Tl_3VSe_4, Science **360**, 1455 (2018).

[71] S. E. Kim and D. G. Cahill, Pushing low thermal conductivity to the limit, Science **373**, 963 (2021).

[72] A. Einstein, Elementare betrachtungen über die thermische molekularbewegung in festen körpern, Ann. Phys. (Leipzig) **340**, 898 (1911).

[73] D. G. Cahill, S. K. Watson, and R. O. Pohl, Lower limit to the thermal conductivity of disordered crystals, Phys. Rev. B **46**, 6131 (1992).

[74] M. T. Agne, R. Hanus, and G. J. Snyder, Minimum thermal conductivity in the context of diffuson-mediated thermal transport, Energy Environ. Sci. **11**, 609 (2018).

[75] Y.-F. Ding, Z.-L. Yu, P.-B. He, Q. Wan, B. Liu, J.-L. Yang, and M.-Q. Cai, High-Performance Photodetector Based on $InSe/Cs_2XI_2Cl_2$ (X= Pb, Sn, and Ge) Heterostructures, Phys. Rev. Appl. **13**, 064053 (2020).

[76] H. Li, T. Luo, S. Zhang, Z. Sun, X. He, W. Zhang, and H. Chang, Two-dimensional metal-halide perovskite-based optoelectronics: synthesis, structure, properties and applications, Energy & Environmental Materials **4**, 46 (2021).